Comparative Study of Mechanical And Corrosion Properties of Coating on the Basis of ZrN and TiN Solid Solutions

N.N. Cherenda [1]*, S.N. Grigoriev[2], A.V. Basalai[3], A.B. Petukh[4], A.A. Vereschaka[5], O.V. Reva[6], A.Yu. Isobello[3], D.P. Rusalsky[1], A.K. Kuleshov[1], V.V. Uglov[1]

[1]Belarusian State University, Nezavisimosti ave. 4, 220030 Minsk, Belarus;
[2]Moscow State University of Technology “STANKIN”, Vadkovsky Lane 3a, 127055 Moscow, Russia;
[3]Physical Technical Institute of the National Academy of Sciences of Belarus, Kuprevicha str. 10, 220141, Minsk, Belarus;
[4]A.V.Lykov Heat and Mass Transfer Institute of the National Academy of sciences of Belarus, P. Brovka str. 15, 220072 Minsk, Belarus;
[5]Institute of Design and Technological Informatics of the Russian Academy of Sciences (IDTI RAS), Vadkovsky Lane 18a, 127055 Moscow, Russia;
[6]Department of Chemical, Biological, Radiation and Nuclear Protection of the State Educational Institution "University of Civil Protection" of the Ministry of Emergency Situations of the Republic of Belarus, Mashinostroiteley street, 25, 220118, Minsk, Belarus;

*****Correspondence: Tel.: +375172095590; Fax: +3752095445; E-mail: cherenda@bsu.by

Abstract: ZrN, (Zr,Ti)N, (Zr,Hf)N, (Zr,Nb)N, (Ti,Zr,Hf)N and (Ti,Zr,Nb)N coatings mechanical and corrosion properties were investigated in this work. Coatings were deposited by vacuum arc deposition technique on Ti-6Al-4V titanium alloy. Microhardness measurements, tribological and scratch tests, profilometry, electrochemical corrosion tests, scanning electron microscopy were used as investigation techniques. The highest microhardness value (36.2 GPa) was observed for (Zr,Hf,Ti)N coating, and the lowest value (12 GPa) - for (Zr,Nb)N coating. The highest critical forces Lc3 during scratch tests were found for coatings containing hafnium. It was revealed that the shape of anodic potential dependence on time during electrochemical corrosion tests in galvanostatic mode (3% NaCl environment) strongly dependent on coating type. The time necessary to reach the maximum stable value of anodic potential can be an indirect parameter of corrosion resistance. (Zr,Nb,Ti)N coating demonstrated the best corrosion resistance in used test regimes.

Keywords: titanium alloy; medical implants; nitride coating; friction coefficient; adhesion; microhardness, corrosion

1. Introduction

Metal implants are actively used in various fields of medicine (osteosynthesis, dentistry, endoprosthetics, etc.) and titanium alloys being the most frequently used material for such implants (Annur et.al, 2023; Brunello et al.; 2018; Chen and Thouas, 2015; Cordeiro et.al, 2017; Kaur and Singh, 2019; Liu et.al, 2017; Sarraf et.al, 2023). Unfortunately, complications in the form of soft tissue inflammation around metal implants often occur when using these products. This refers to the formation of a wound channel in the soft tissues and bone around the inserted implant. These wounds can serve as a source of microbial contamination with a corresponding reaction of the body in the form of simple tissue infiltration around the implant, purulent inflammation or spoke osteomyelitis. Impants as prosthetic elements introduced into the body are foreign bodies (corpora aliena) and can cause a corresponding reaction of the immune and other systems of the human body (Kaur and Singh, 2019). For example, Ti-6Al-4V alloy, that is widely used for implants production, contains potentially toxic atoms of aluminum and vanadium (Chen and Thouas, 2015; Nouri and Wen, 2015; Khorasani et al., 2015; Kaur and

Singh, 2019; Chen et al., 2023) which have the risk of releasing into the human body. Vanadium has been associated with gastrointestinal discomfort and decreased body weight gain, carcinogenic effect (Kaur and Singh, 2019). Aluminium is also toxic in high doses and can be linked to a number of diseases: neurotoxicity, impairment of motor functions, reduction of spatial memory capacity and Alzheimer's disease (Kaur and Singh, 2019).

There are several ways to avoid this negative effect. Application of different surface modification techniques e.g. deposition of protective coatings is one of approaches most widely used (Gabor et al., 2024, Rabadzhiyska et al., 2024; Grigoriev et al., 2023a). Modification of the surface properties of the implant material using coatings deposited using various methods can significantly reduce the risk of occurrence and development of the above complications, and can significantly accelerate the healing process and reduce the labor intensity of implant maintenance. Deposition of modifying coatings on the surface of implants allows them to be given the necessary properties for biological, physical and chemical inertness, and to achieve complete elimination of the possibility of metallosis. Besides that coating deposition can reduce corrosion electrochemical processes, and, consequently, allow achieving a reduction or complete elimination of allergic and toxic-chemical reactions (Huang et al., 2019; Mohamadian Samim et al., 2021; Rabadzhiyska et al., 2024).

ZrN films and coatings possess good mechanical and biological properties, good corrosion resistance making them applicable in bioengineering and industry (Laera et al., 2021; Lamm et al., 2023; Rabadzhiyska et al., 2024; Tang et al., 2016). ZrN coatings are commercially available coatings for orthopaedic implants, which are used for articulating surfaces in joint arthroplasty (Gabor et al., 2024). The properties of ZrN coatings can be improved with the deposition of multilayered metal nitride systems (Gabor et al., 2024). Multilayer nanoscale coatings on the basis of nitrides of transition metals are well-known for their unique physical-mechanical properties, as well as good corrosion resistance (Chen et al., 2020; Dohm et al., 2024; Frank et al., 2022; Gabor et al., 2024; Lotkov et al., 2021; Mohamadian Samim et al., 2021; Pogrebnjak et al., 2017; Wu et al., 2022). In particular, ZrN/TiN multilayer coatings exhibited a higher fracture stress compared to the single-layer coatings (Frank et al., 2022). In (Mohamadian Samim et al., 2021) it was reported that corrosion resistance of ZrN/CrN nanolayers is enhanced by increasing the number of bilayer periods thus blocking the penetration path of corrosive solution. Even penetration of hydrogen through the coating can be slowed down in such a way (Lotkov et al., 2021).

Investigations carried out earlier revealed the phase-structural characteristics of ZrN, (Zr,Ti)N, (Zr,Hf)N, (Zr,Nb)N, (Ti,Zr,Hf)N and (Ti,Zr,Nb)N single layered and multilayered coatings which were deposited using one or two cathodes on a Ti6Al-4V titanium alloy substrate by means of physical vapor deposition (Vereschaka et al., 2023). Different types of corrosion tests including placement in 1M solutions with acidic (H_2SO_4), alkaline (NaOH) and neutral (NaCl) media at a constant temperature of 50 °C as well as forced electric potential tests showed high corrosion resistance of all coatings. However it was found that the difference in corrosion characteristics was negligible. Investigations of mechanical properties of the above mentioned coatings (microhardness, friction coefficient, coatings adhesion) as well as additional corrosion testing in a 3% NaCl environment to find the influence of the coatings composition and structure on their behavior in a corrosive environment were the main aims of this work.

2. Experimental

The samples of Ti-6Al-4V titanium alloy (Grade 5) were used for investigations. The diameter of the samples was 25 mm, their thickness – 3 mm. The samples were mechanically grinded before plasma treatment. The parameters of the surface roughness and waviness were equal to: R_a=0.4 μm, R_z=4.1 μm, W_a= 0.24 μm. Roughness parameters of samples corresponded to roughness parameters of workpieces used for production of hip joints parts.

Coatings were deposited by vacuum arc deposition technique with controlled movement of cathode spot in nitrogen atmosphere using a modernized VIT-2 PVD installation (Grigoriev et al., 2023b; Vereschaka et al., 2020). Cleaning of the surface by Zr ions was carried out before deposition resulting in formation of thin (~ 50 nm) metal sublayer. The coatings were deposited using one or two metal cathodes. The following cathodes were used: Zr, Ti, 50 at.% Zr - 50 at.% Nb, 50% at. Zr – 50 at.% Hf. As a result, the following coatings were deposited: ZrN, (Zr,Nb)N, (Zr,Hf)N, (Zr,Ti)N, (Zr,Hf,Ti)N and (Zr,Nb,Ti)N.
Earlier conducted investigations have shown that single-phase coating on a basis of ZrN solid solution were formed using one Zr-containing cathode (Vereschaka et al., 2023). Using two cathodes (a Zr-containing cathode and a Ti cathode) a two-phase coating containing solid solutions on a basis of ZrN and TiN was formed (Vereschaka et al., 2023). Elemental composition of coatings is shown in Table 1. Coatings thickness was about 2.5 μm.

Table 1. Concentration of elements in coatings

Coating	Elements concentration, at.%				
	Ti	Zr	Nb	Hf	N
ZrN	-	48,7	-	-	51,3
(Zr,Nb)N	-	23,5	23,4	-	53,1
(Zr,Hf)N	-	43,5	-	5,7	50,8
(Zr,Ti)N	22,2	30,5	-	-	47,3
(Zr,Nb,Ti)N	37,0	7,5	7,5	-	48,0
(Zr,Hf,Ti)N	22,5	26,6	-	3,4	47,5

The microhardness of the coatings was determined on an automated microhardness tester Duramin 5 (Struers, Denmark) by the indentation method using a Knoop indenter. The normal load on the diamond indenter was 0.5 N, the holding time in the loaded state was 10 s.
Tribological tests were carried out on a UIPT-001 tribometer (Belarus) under dry friction conditions with reciprocating motion of an indenter made of hard alloy (WC – 92 %, Co – 8 %). The indenter speed was 2 mm/s, the load on the indenter was 0.5 N. The tests were carried out at room temperature with a relative air humidity of 40%-50%.
Surface topography was characterized using Mahr MarSurf SD 26 profilometer (Germany). The length of the track was 17 mm, length of base line for calculation of roughness and waviness parameters was 5.7 mm. Ra parameter (the average arithmetic deviation of the profile) was averaged after measurements on 6 tracks. Data were processed using a software package MarSurf XR 1.
Scratch tests were carried out with 0.4 mm radius diamond indenter with a load linearly increasing from 0.05 to 98 N. The scratch tracks length was 15 mm (loading speed 0.17 kg/s, sample movement speed 0.19 mm/s) and 7.5 mm (sample movement speed 11.5 mm/min). Three tests were carried out on each sample.
Corrosion tests of nitride coatings were carried out on an Autolab/PGSTAT302N potentiostat-galvanostat (Metrohm Autolab B.V., Utrecht, Holland) in a galvanostatic mode. In this mode a constant current load of 4 mA was applied to coating (anode) and change of potential in time was recorded. The reference electrode was a saturated silver chloride electrode, and the counter electrode was a platinum plate. The working surface area of each coating was 1 cm^2. All tests were carried out in a solution of 3% NaCl at room temperature and without convection. Analysis of elemental composition and surface morphology of coatings areas after corrosion tests were carried out by scanning electron microscopy (SEM) using TESCAN MIRA 3 LMH (Tescan, s.r.o., Czech Republic) and LEO1455VP (Karl Zeiss, Germany) microscopes.

3. Results and Discussion

Mechanical properties

Figure 1 shows the results of microhardness measurements for all types of coatings under a load of 0.5 N. The indentation depth was varied from 0.45 to 0.79 μm during measurements, i.e. the indenter penetration depth was less than the coating thickness. As one can see from the presented data, the highest microhardness value (36.2 GPa) was observed for samples with a (Zr,Hf,Ti)N coating, and the lowest value (12 GPa) - for samples with a (Zr,Nb)N coating. The microhardness of the samples of the original titanium alloy Ti-6Al-4V was 3.7 GPa. Addition of titanium atoms to the coating leads to an increase in microhardness. A possible reason of this effect is the formation of a layered structure of the coating: alternation of layers of solid solutions on a basis of ZrN and TiN. Such a layered structure of the coatings appeared as a result of rotation of the holder with samples and cyclic change in the distance from the surface of the samples to each of the cathodes. In addition, the microhardness of the TiO_2 dioxide coating, which is used for components of commercial endoprostheses introduced into clinical practice, was measured. The microhardness of the Ti-6Al-4V samples with a titanium dioxide coating was 4.9 GPa.

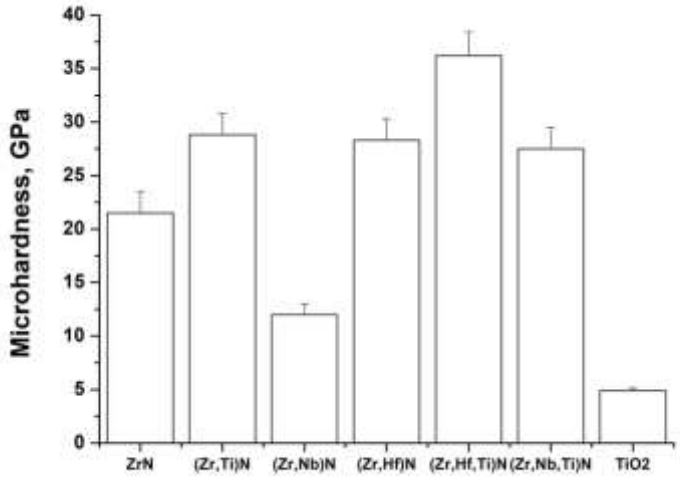

Figure 1. Microhardness values of samples with coatings

The tribological tests showed that the friction coefficient values for all coatings was varied in the range of 0.15-0.17 (Figure 2). All coatings have a higher coefficient of friction than that of the substrate material in conditions of used tribological tests. The value of the friction coefficient is determined by a number of factors. Some of the most significant are the strength characteristics of the material under study and the roughness of its surface. Comparison of the data presented in Figures 1 and 2 showed that addition of titanium atoms into the coating led to microhardness growth and can also led to a decrease in the friction coefficient (e.g. compare pairs of coatings (Zr,Nb)N and (Zr,Nb,Ti)N or (Zr,Hf)N and (Zr,Hf,Ti)N). However, for some pairs of coatings, an inverse relationship was also observed (e.g. (Zr)N and (Zr,Ti)N), which may be due to the influence of other prevailing factors.

Friction coefficient data correlate with previously obtained data on surface morphology observed by scanning electron microscopy (Vereschaka et al., 2023). In particular, it was found that the highest friction coefficient values corresponded to coatings that were characterized by a larger amount of droplet phase on the surface, which may be associated with increased adhesion between the indenter and the metal droplet phase.

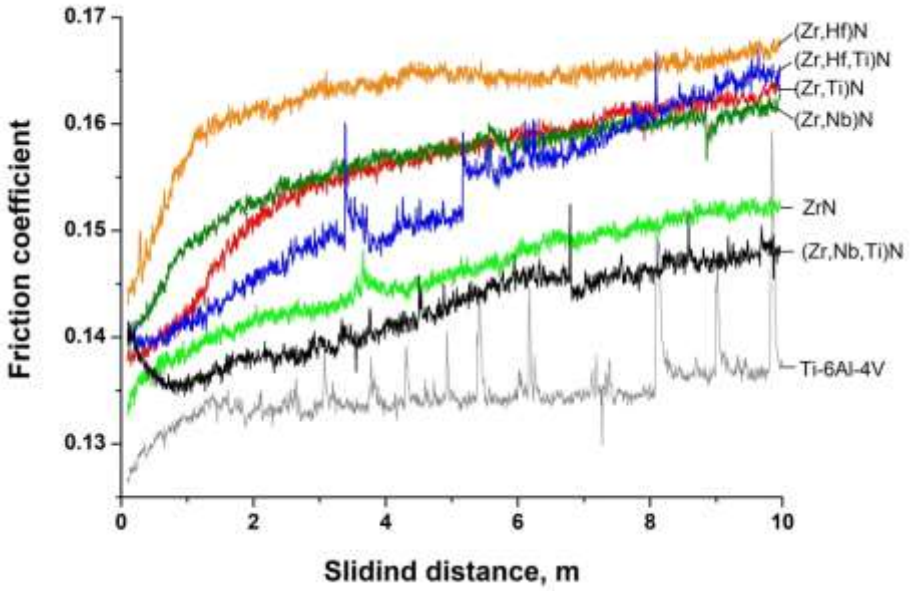

Figure 2. Dependence of coatings friction coefficient on the sliding distance

In order to study the influence of surface morphology on the friction coefficient, the parameters of surface roughness were determined. Figure 3 shows the values of Ra obtained using a profilometer. Measurements were taken along and across the direction of samples grinding.

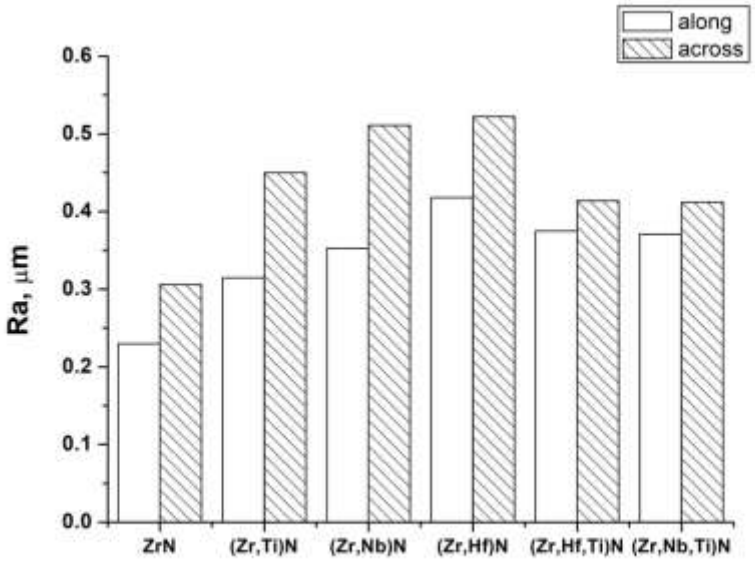

Figure 3. Ra values of coatings measured along and across the grinding direction

It is evident from Figure 3 that the values of the average arithmetic deviation of the profile are smaller when measured along the grinding direction for all samples. Their value varied from 0.23 to 0.41 μm. The values of the Ra parameter measured across the grinding direction were within 0.3-0.6 μm. The roughness of the coating surface will be significantly determined by its morphology - the presence of a droplet phase and other surface inhomogeneities. In particular, one can see that for the (Zr,Hf)N coating, higher Ra values were observed both along and across the surface, which may be due to the larger size of the droplet phase, which correlated with the

data of tribological tests and scanning electron microscopy (Vereschaka et al., 2023). Besides that it can be seen from the Figure 3 that the Ra value of the (Zr,Ti)N coating was higher than that of the ZrN coating, which may be the reason for the increase in the friction coefficient (Figure 2).

After coatings deposition on the titanium alloy tests were also conducted on their adhesive strength. All scratches were made along the direction of samples grinding. Investigations showed that the tracks were characterized by the appearance of chips on the sides of the track, and subsequent full delamination of the coating. It is known that three main critical loads are usually determined using scratch tests: Lc1 corresponding to initial cracking appearance, Lc2 – first chipping and Lc3 – full delamination of a coating (Randall, 2019). In these experiments the critical forces Lc2 and Lc3 were determined using optical microscopy basing on the distance at which chipping and delamination occurred and basing on the dependence of the load applied on the diamond indenter sliding distance. The Table 2 shows the critical normal force, determined using optical microscopy, at which the first chipping and complete delamination of the coating were observed. The obtained data show some correlation between the critical force at which complete delamination of the coating occured and the critical force at which the first chips were observed along the track.

Table 2. Critical normal force corresponding to the first appearance of chips (Lc2) and complete delamination (Lc3) of coatings

Coating	Lc2, N	Lc3, N
ZrN	24.5	37.3
(Zr,Ti)N	17.7	26.5
(Zr,Nb)N	14.7	33.4
(Zr,Hf)N	29.4	54.0
(Zr,Hf,Ti)N	20.6	41.2
(Zr,Nb,Ti)N	19.6	24.5

Another criterion for full delamination of coating deposited on a relatively smooth surfaces may be a sharp change in the value of the friction coefficient of the diamond indenter during sctratch tests (Cherenda et al., 2024). The dependences of the friction coefficient of the indenter on it sliding distance are shown in Figure 4. The dependences show a sharp increase in the friction coefficient indicating full delamination of the coating and penetration of indenter into Ti-6Al-4V alloy, that corresponds to the values of critical force Lc3 obtained using optical microscopy.

Besides that, one can see from the Figure 4 that the friction coefficient of the (Zr,Hf)N coating (friction path area 2-5 m) is greater than the friction coefficient of the (Zr,Nb)N and ZrN coatings, that confirms the dependencies presented earlier (Figure 2).

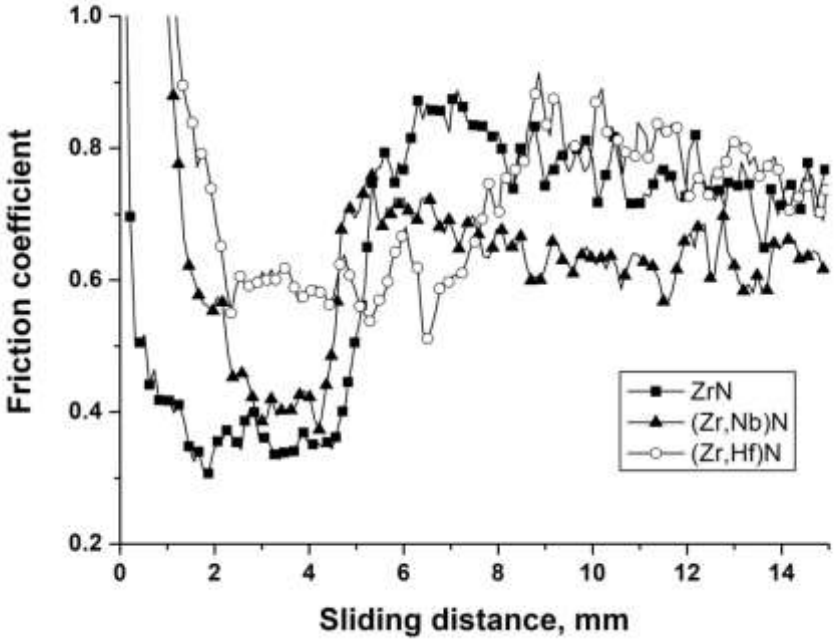

Figure 4. Dependence of the coatings friction coefficient of a diamond indenter on its sliding distance

The highest critical force Lc3 was observed for samples with coatings containing hafnium: (Zr,Hf)N and (Zr,Hf,Ti)N. The (Zr,Hf)N coating also demonstrated the highest value of the critical force Lc2. However, as can be seen from the images of areas where coating delamination occured (Figure 5), these coatings are characterized by the largest chips along the entire length of the track, compared to the other coatings.

a)

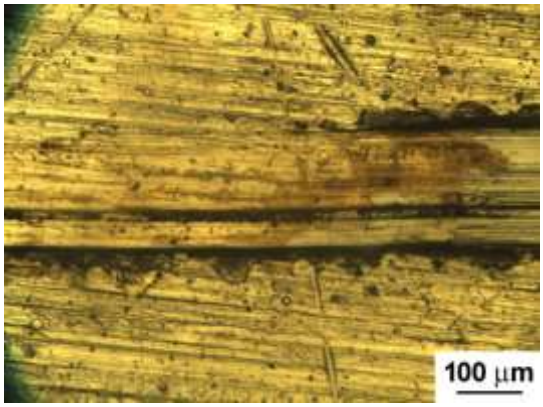

b)

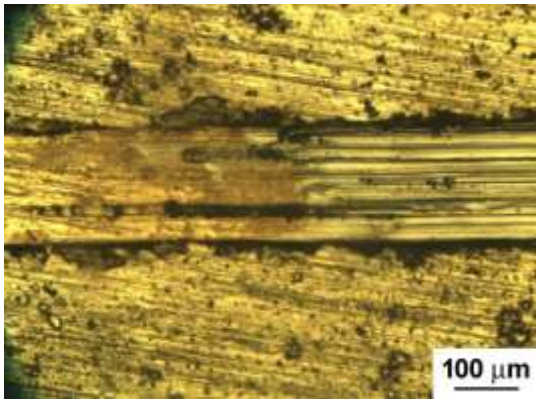

c)

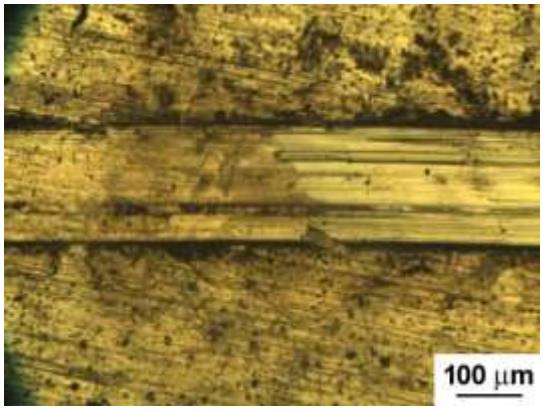

d)

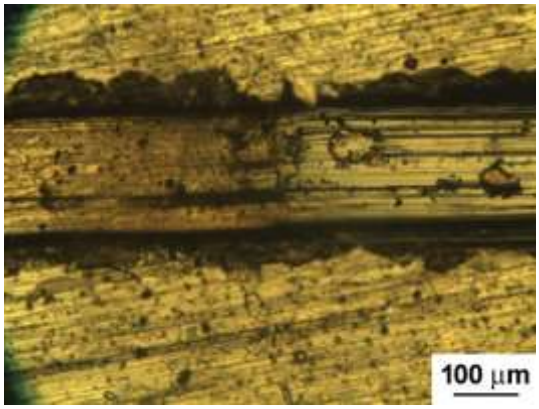

e)

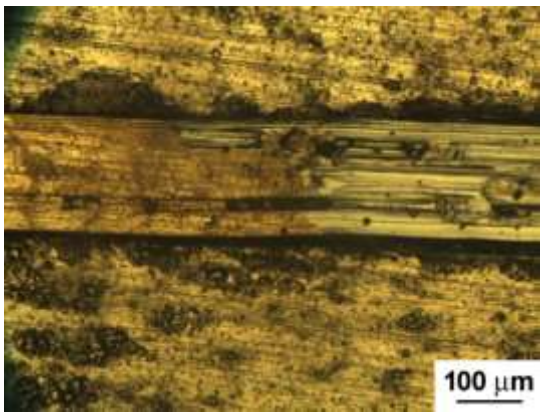

f)

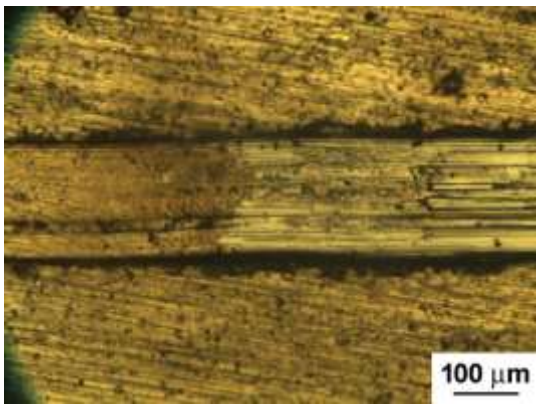

Figure 5. Surface morphology (optical microscopy) of coated samples at the areas of coatings full delamination: ZrN (a), (Zr,Ti)N (b), (Zr,Nb)N (c), (Zr,Hf)N(d), (Zr,Hf,Ti)N(e), (Zr,Nb,Ti)N (f).

It should be noted that coatings containing Nb showed relatively small values of critical loads, which may be associated with the presence of tensile stresses in the ZrN solid solution (Vereschaka et al., 2023), which contribute to the destruction of the coating during tests.

Corrosion properties

Previous investigations have shown that the studied protective coatings have high corrosion resistance at various temperatures and in various aggressive environments, including body fluids (Vereschaka et al., 2023). At the same time, number of corrosion characteristics determined in experiments were practically independent of the type of coating. In order to find the influence of the composition on coatings behavior in a corrosive environment additional studies of corrosion resistance were carried out in a 3% NaCl environment in galvanostatic mode at a high constant current load of 4 mA.

Figure 6 shows the dependences of the anodic potential of some tested coatings on time. One can see from the figure that a sharp increase of potential was observed at the beginning of the tests, which may be associated with the formation of passivating films on the surface. Then, the potential was diminished and a temporary section of its relatively constant value was observed. After that a sharp or gradual growth to a relatively constant value of 2.1-3.4 V was occurred. Dependencies for ZrN and (Zr,Hf)N coatings were similar to that of (Zr,Nb)N in the shape (Figure 6).

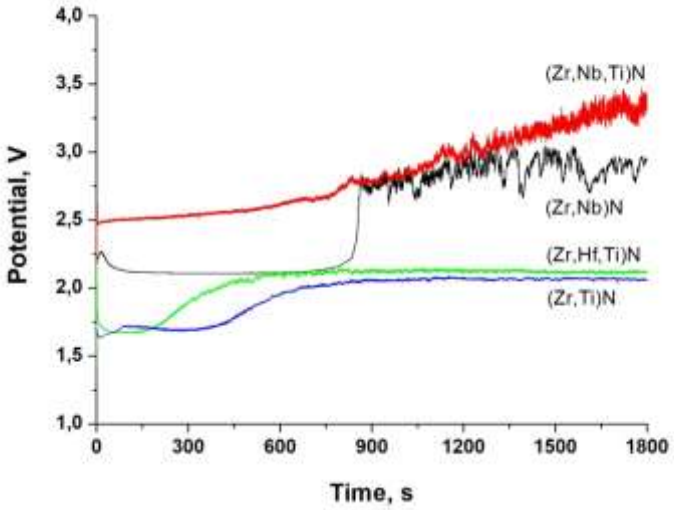

Figure 6. Dependence of the anodic potential on time for coatings (ZrTi)N, (Zr,Nb)N, (Zr,Hf,Ti)N and (Zr,Nb,Ti)N coatings.

An aqueous solution of 3% NaCl corresponds to a concentration of 0.5 mol/l and differs little in electrochemical characteristics from a standard 1M solution, as shown by calculations using the Nernst equation. Thus, the process of oxidation of chlorine ions occurring at the anode at room temperature and atmospheric pressure is characterized by following equations:

$$2Cl^- - 2e^- = Cl_2\uparrow \quad E= E^0 + 0.059/2 \lg(0.5) = 1.358 + 0.0295 \cdot 0.29 = 1.3665 \text{ V}$$

where E is equilibrium potential, E^0 is standard potential.
In a neutral aqueous solution, the anodic process of oxygen evolution is also possible:

$$2H_2O - 4e^- = O_2\uparrow + 4H^+; \; E = 1.23 \text{ V}$$

The potential onset of corrosion processes on the presented curves is just close to these values, which is obviously associated with the release of gaseous chlorine on the anode. Chlorine is a very strong oxidizer and corrosive agent in an aqueous medium, which reacts with almost all metals and metalloid elements. Oxygen, the release potential of which is lower, obviously does not interact with chemically stable nitrides, but may be connected to the corrosion process when the titanium substrate is exposed.
Since the materials being tested are not pure metals, but stable nitride composites of zirconium, hafnium, niobium and titanium in various combinations on a titanium substrate, they corrode for a fairly long time (up to ~ 1700 s) - until the potential reaches its maximum value. However, as the concentration of chlorine in the aqueous solution in the anode zone increases, the process of its disproportionation is activated:

$$Cl_2 + H_2O \leftrightarrow HOCl + HCl$$

Under normal conditions, about a third of the dissolved chlorine is hydrolyzed, therefore the concentration of hypochlorous acid gradually increases in the system. Hypochlorous acid is a very strong oxidizer (the largest among oxygen-containing acids of chlorine) and is capable of decomposing in solution with the formation of atomic oxygen by a radical mechanism and chlorine oxide through the short-lived radical $ClO^\bullet$. Hypochlorous acid in solution is capable of parallel independent transformation of three types:

$$HClO \leftrightarrow HCl + O^\bullet$$
$$2HClO \leftrightarrow H_2O + Cl_2O$$
$$3HClO \leftrightarrow 2HCl + HClO_3$$

The conversion potentials of HClO at the anode in the presence of water range from 0.8 to 1.6 V, so when a certain concentration is reached, all these forms in the solution can actively participate in the destruction of both the studied nitride coatings and the titanium substrate.
In addition, the above processes can be intensified in an alkaline environment, which is formed in the cathode zone of the NaCl solution, gradually spreading throughout the entire volume of the liquid, since sodium ions from an aqueous solution are not reduced by electric current:

$$\text{cathode: } 2H_2O + 2e^- = H_2 + 2OH^-$$
$$\text{summary process: } 2H_2O + 2NaCl = H_2\uparrow + 2NaOH + Cl_2\uparrow$$

A sharp increase in potential on the dependence of anodic potential on time (Figure 6) is associated with the beginning of active anodic destruction of the substrate material and its

numerical value is associated with the nature of the coating (Table 3). A sharp increase up to the maximum value was characteristic for coatings ZrN, (Zr,Hf)N and (Zr,Nb)N deposited from one cathode, while a gradual exit to the maximum value was observed for coatings (Zr,Ti)N, (Zr,Hf Ti)N and (Zr,Nb,Ti)N obtained from two cathodes. Such behavior may be explained by the fact that the use of two different cathodes led to the formation of coatings consisting of alternating layers of varied composition Each of the compositions has its own corrosion characteristics, therefore for multilayer coatings no sharp transition was observed from the predominant dissolution of the coating to the dissolution of the substrate material.

Table 3. Maximal potentials and time of active dissolution of coatings

Coating	Maximum potential, V	Dissolution time, s
ZrN	2.1	1000
(Zr,Ti)N	2.08	900
(Zr,Hf)N	2.3	1450
(Zr,Nb)N	2.8	850
(Zr,Hf,Ti)N	2.1	750
(Zr,Nb,Ti)N	3.4	1700

If one assume that potential values presented in the Table 3 corresponded to complete or partial corrosion destruction of the coating, then the time to reach this value can be an indirect parameter of corrosion resistance. Analysis of the results showed that the coating (Zr, Hf)N had the greatest resistance to corrosion among single-phase coatings, and (Zr, Nb,Ti)N - among two-phase coatings according to this parameter.

Under standard conditions in aqueous solutions, the concentration of the active agents formed is quite low, but with a constant forced electrochemical process it gradually becomes sufficient to destroy the nitride coatings with the formation of ulcerous, crevice and point lesions. Therefore, additional studies of coatings areas subjected to electrochemical corrosion tests were carried out using SEM. Figure 7 shows the surface morphology of the coatings after the completion of corrosion tests.

a) b)

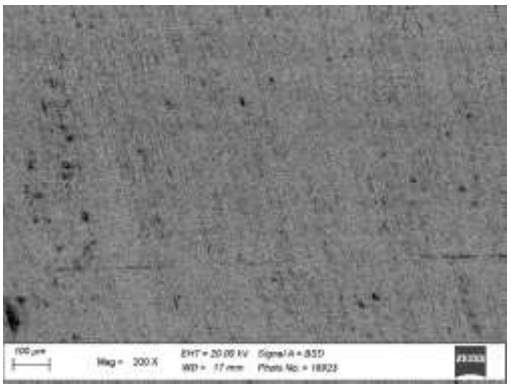

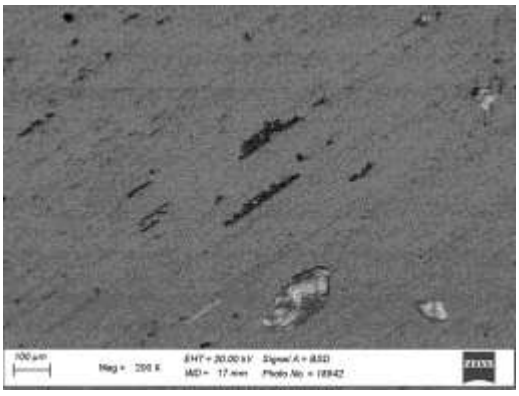

c)

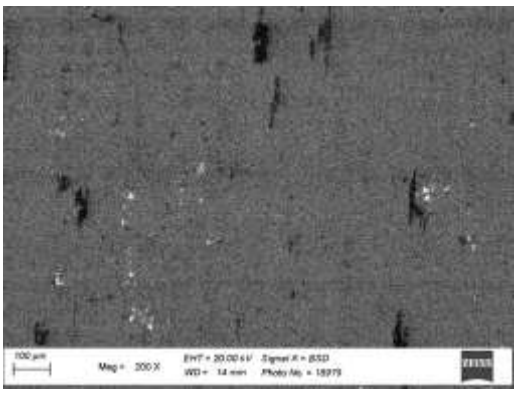

d)

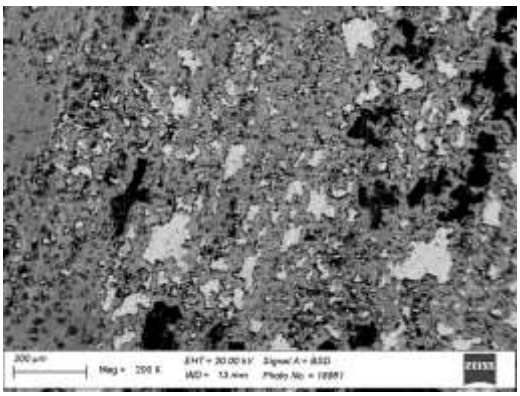

e)

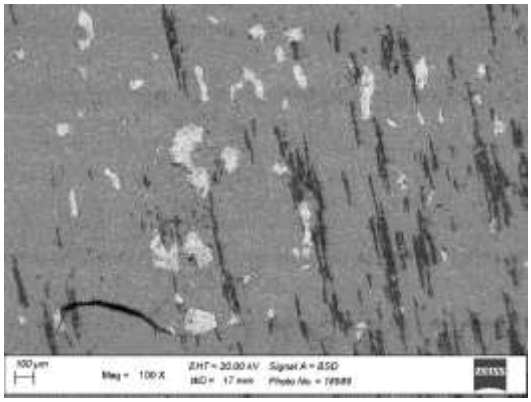

f)

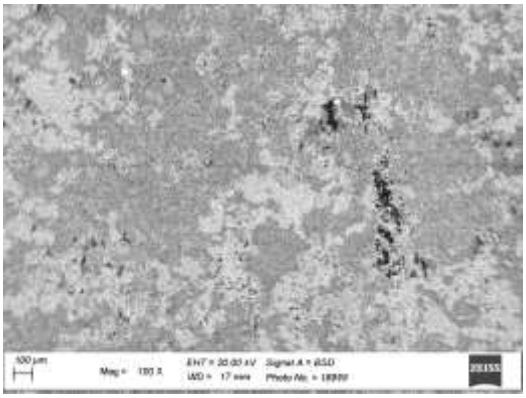

Figure 7. Surface morphology of coatings areas after completion of corrosion tests: ZrN (a), (Zr,Ti)N (b), (Zr,Hf)N (c), (Zr,Nb)N (d), (Zr,Hf,Ti)N (e), (Zr,Nb,Ti)N (f)

One can see from Figures 6 and 7 that a sharp change in the value of the anodic potential corresponded to the formation of a more homogeneous surface morphology and, as a rule, to the complete dissolution of the coating on the studied area. At the same time, a gradual change in the value of the potential corresponded to the surface morphology containing areas of different elemental composition (the contrast in the image was formed by backscattered electrons), i.e. undissolved areas of the coating.

More detailed studies of the areas subjected to corrosion showed that for the case of the ZrN coating (under the conditions of the corrosion tests) there were practically no traces of the coating on the surface (Figure 7a). These areas contained traces of corrosion of the titanium alloy with an increased oxygen content. Such corrosion traces were observed for all types of coatings and have the form of dark spots of irregular shape (Figure 8).

a)

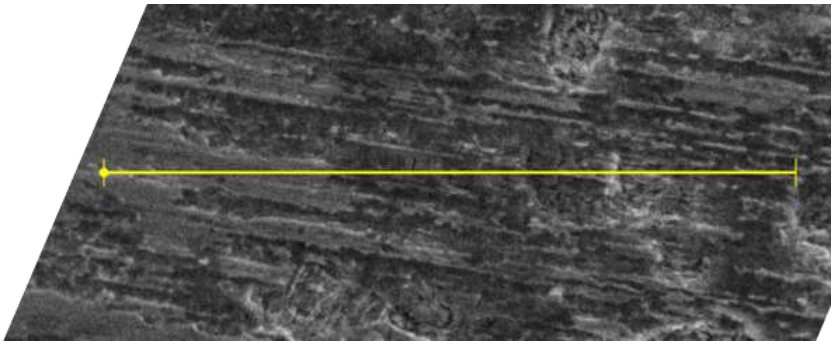

b)

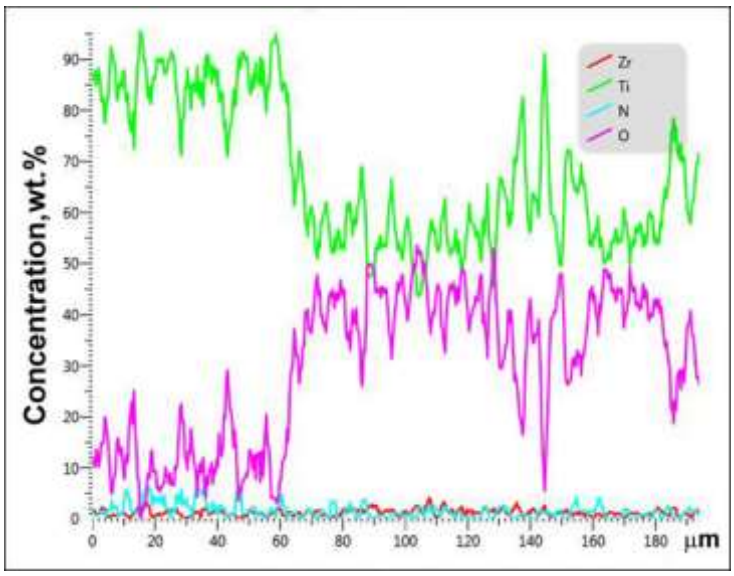

Figure 8. Surface morphology (a) and elements distribution along the line (b) for an area of the sample with ZrN coating subjected to corrosion.

For the case of the (Zr,Hf)N areas of undissolved coating were observed on the surface (Figure 9). As in the previous case, area in Figure 9 contained traces of corrosion of the titanium alloy with an increased oxygen content. For these two types of coatings, a sharp increase of potential up to a maximum values of 2.1-2.3 V was observed, which, according to the data obtained, corresponded to corrosion of the substrate material itself.

a)

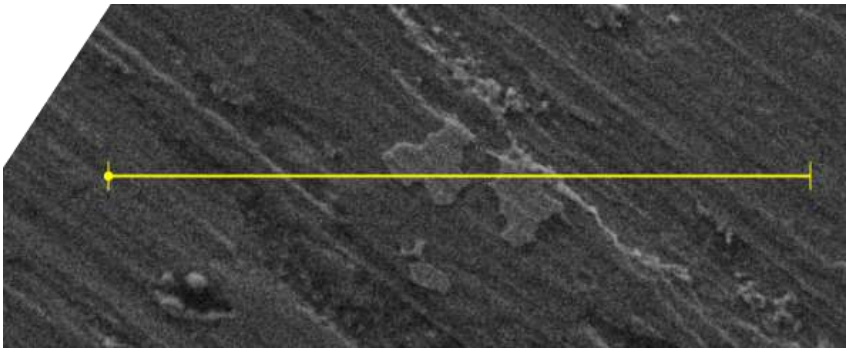

b)

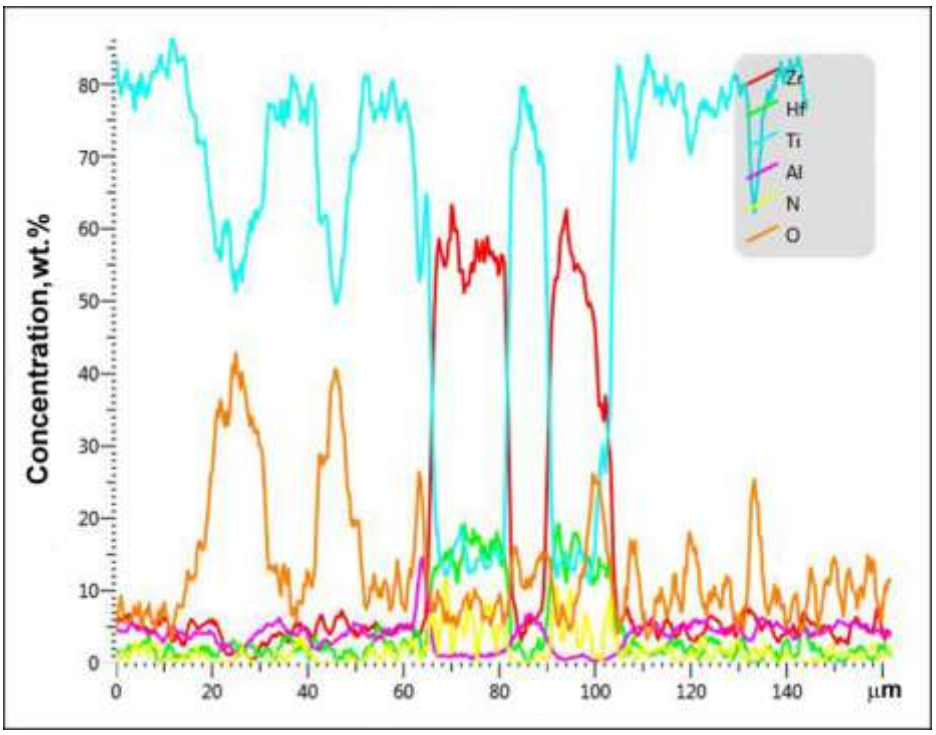

Figure 9. Surface morphology (a) and elements distribution along the line (b) for an area of the sample with (Zr,Hf)N coating subjected to corrosion.

The complication of the coating composition and its architecture led to corrosion resistance increase. In particular, the addition of titanium atoms to the ZrN coating led to a growth of number of areas with undissolved coating (Fig. 7b). Similar effect was observed after the addition of titanium atoms to the (Zr, Hf)N coating (Fig. 7e). For a coating of a more complicated composition, this effect was more pronounced. In particular, the combined use of Ti and Zr-Nb cathodes for spraying the (Zr,Nb,Ti)N coating provided (under the conditions of the tests) the best continuity of the coating on the surface of the test area (Figure 10). Elements of this coating were predominantly observed over the entire surface of the investigated area. One can see from Figure 10 that the areas of undissolved coating had different thicknesses. Traces of titanium alloy corrosion were also observed on the surface. For this coating a gradual increase of potential was observed (Figure 6), and the maximum potential value more likely was not reached. Thus (Zr,Nb,Ti)N coating that had the best resistance to forced electrochemical corrosion among the studied types of nitride coatings (under the conditions of this experiment). It should be noted that used corrosion regimes were significantly more severe than regimes that could be established in the liquid environments of the human body. So applied corrosion regimes are more suitable for corresponding industrial applications of these nitride coatings.

a)

b)

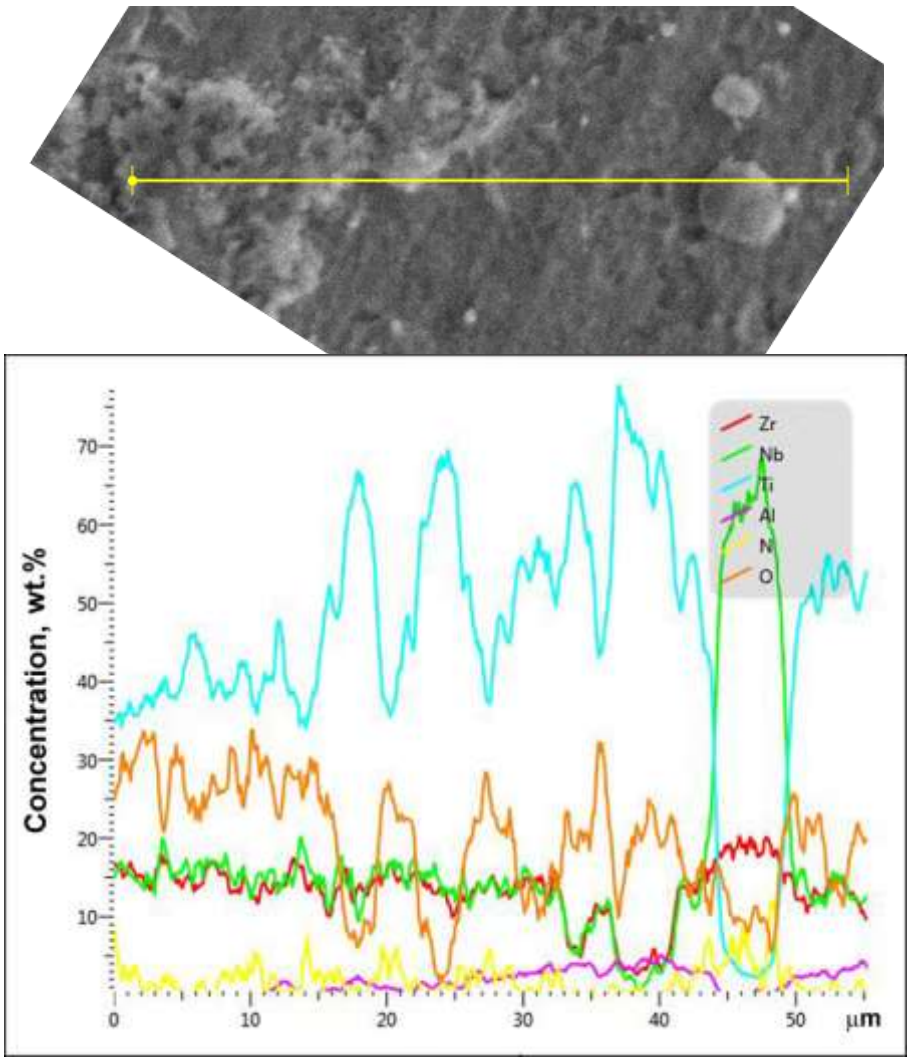

Figure 10 - Surface morphology (a) and distribution of elements along the line (b) for an area of the sample with a (Zr,Nb,Ti)N coating subjected to corrosion

The conducted studies have shown that to assess the resistance of the studied nitride coatings under conditions of electrochemical corrosion in galvanostatic mode combined investigations are necessary, including both an analysis of the patterns of recorded electrical characteristics dependencies, their correlation with chemical reactions occurring on the surface and an analysis of the surface morphology of the areas subjected to corrosion.

Under the conditions chosen for these investigations, it was found that with a constant anodic current of 4 mA in 30 minutes almost complete destruction of nitride coatings occured in most of cases. In order to determine the nature of destruction of the coatings themselves, the corrosion time in the galvanostatic mode was reduced to 400 s. After that, the morphology and elemental composition of the areas subject to corrosion were analyzed. The results of the studies are presented in Figures 11-14.

One can see from Figures 11 and 12, that for ZrN and (Zr,Hf)N coatings, corrosion had pitting nature. Centers of corrosion attack in the surface plane were spherical and penetrate the entire coating thickness in depth. The addition of Hf atoms to the coating composition led to a decrease in the diameters of corrosion traces from ~ 370 µm to ~ 170 µm, leading to diminishing of the substrate material area that was in direct contact with the corrosive environment and increasing the time of full coating dissolution (Table 3). The appearance of corrosion centers can be caused by a droplet metal phase, the density of which on the surface (Vereschaka et al., 2023) correlated with the density of corrosion centers obtained in this work. The interaction of a locally exposed metal surface with aggressive anions (Cl^-) could be the cause of pitting corrosion.

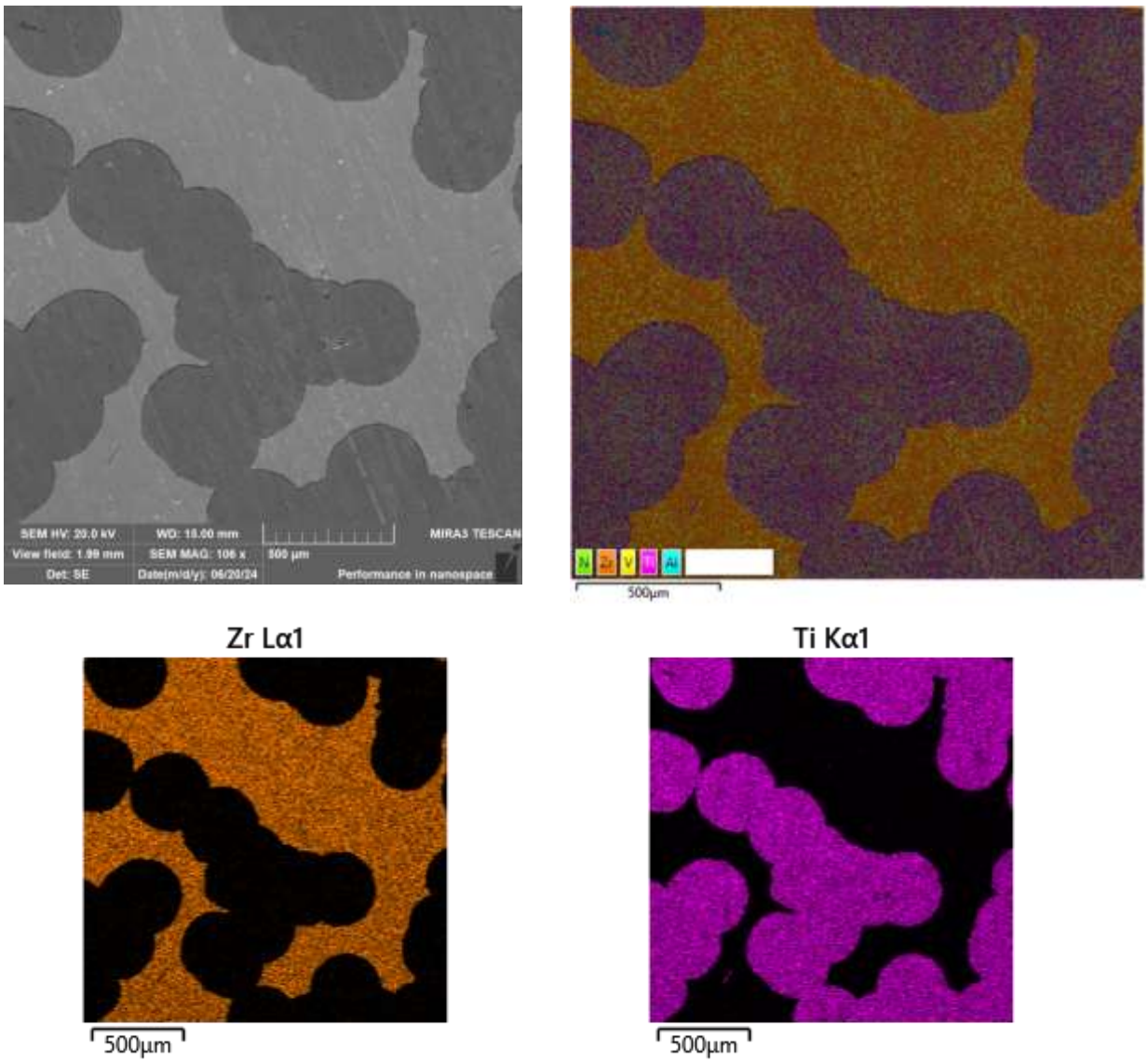

Figure 11. Morphology of the ZrN coating area and elements distribution map after corrosion testing for 400 s.

Earlier it was shown that titanium and titanium alloys are subject to high-temperature rapid corrosion in the presence of chlorides, moreover, the corrosion has a pitting character (Gurappa, 2003). The destruction of the alloy is caused by a reaction with chlorine ions. The following mechanism of corrosion destruction was proposed (Gurappa, 2003). The oxide film formed on the surface is mainly a layer of TiO_2. Titanium oxide reacts with chlorine ions present in the solution, forming $TiCl_2$:

$$TiO_2 + 2Cl^- + 2e^- = TiCl_2 + 2O^{2-}.$$

Chlorine gas reacts with metallic titanium and titanium chloride reacts with oxygen:

$$Ti_{(solid)} + 2Cl_{2(gas)} = TiCl_4$$
$$TiCl_{4(solid)} + O_{2(gas)} = TiO_{2(solid)} + 2Cl_{2(gas)}.$$

Despite the fact that this model was proposed for gas corrosion at high temperatures, similar reactions can also occur locally in aqueous solutions.

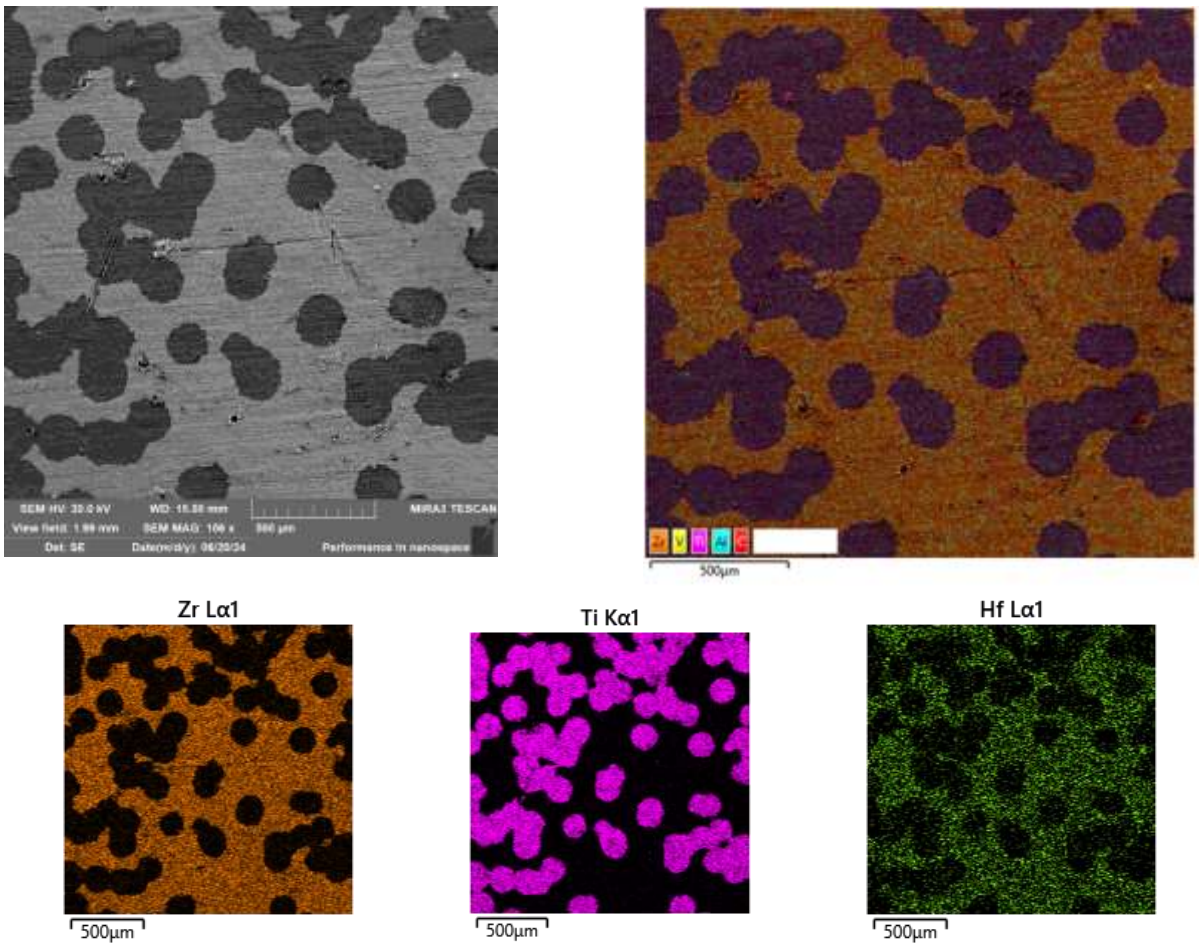

Figure 12. Morphology of the (Zr,Hf)N coating area and elements distribution map after corrosion testing for 400 s.

For other types of coatings, a decrease in the etching time led to an increase in the area of undissolved parts of the coating (Figure 13). That is, in most cases, penetration of the corrosive environment through various types of channels to the substrate material was occurred. As it was found earlier (Zr,Nb,Ti)N coating demonstrated the best result in maintaining the continuity of the surface coating (Figure 14).

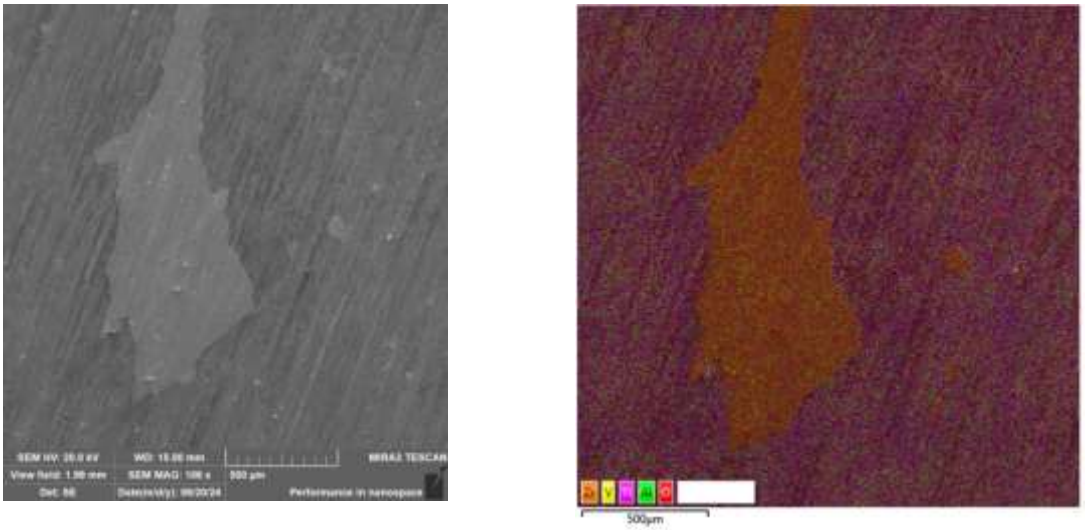

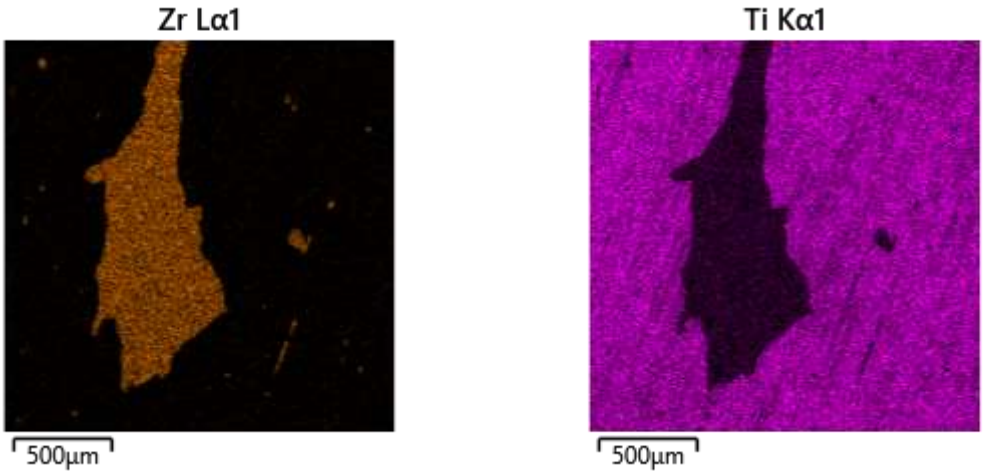

Figure 13. Morphology of the coating area (Zr, Ti)N and elements distribution map after corrosion testing for 400 s.

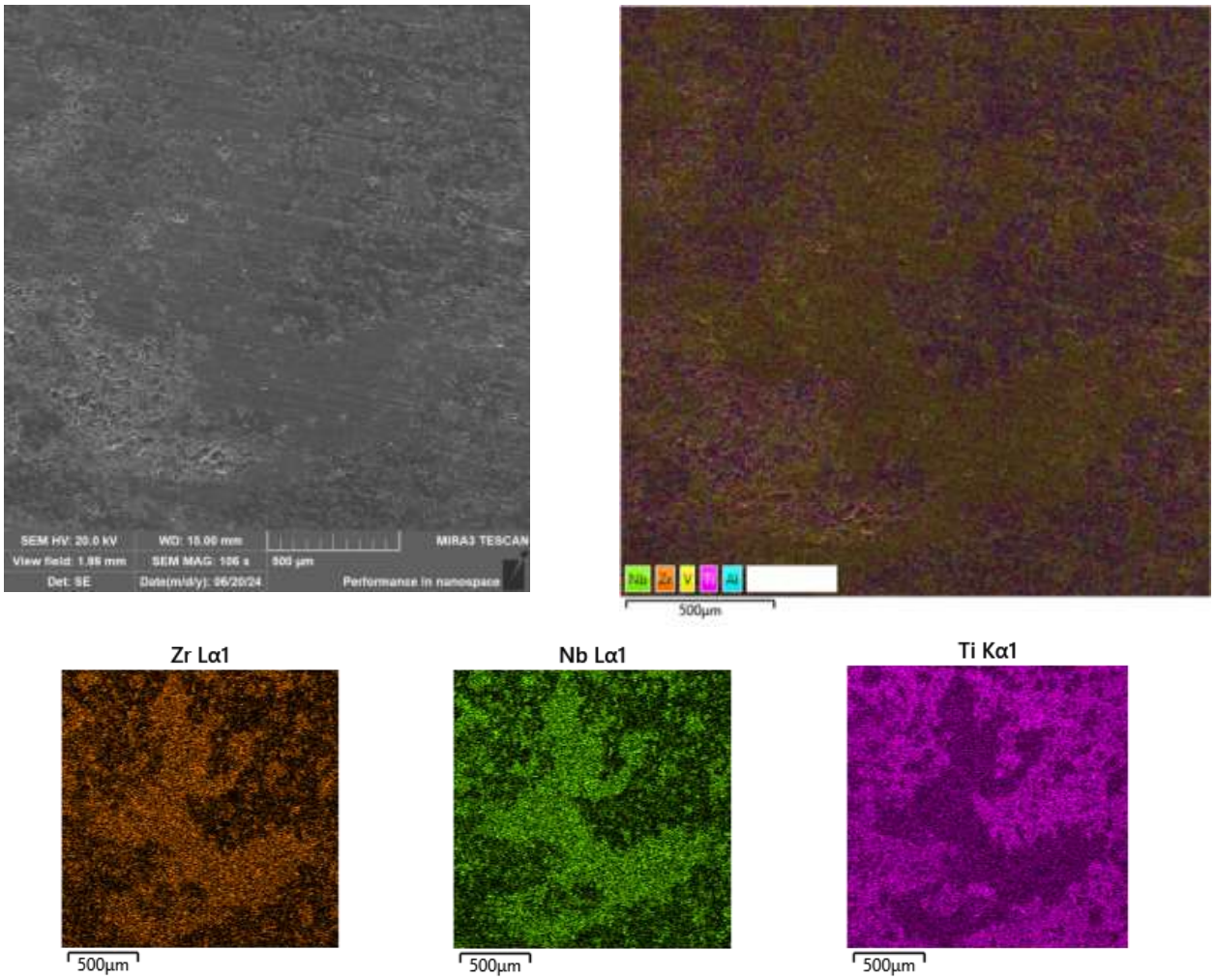

Figure 14. Morphology of the coating area (Zr, Nb, Ti)N and elements distribution map after corrosion testing for 400 s.

Additional studies of coatings on a basis of ZrN and TiN solid solutions, subjected to corrosion tests, allow to determine corrosion character by the difference in dependences of the potential on time, which indicate the occurrence of a number of chemical reactions on the anode surface and

in the near-anode zone with the participation of electrolyte components, leading to an increase in the concentration of chlorine compounds with high corrosion activity over time.

4. Conclusions

Mechanical and corrosion properties of ZrN, (Zr,Ti)N, (Zr,Hf)N, (Zr,Nb)N, (Ti,Zr,Hf)N and (Ti,Zr,Nb)N single layered and multilayered coatings which were deposited using one or two cathodes on a Ti6Al-4V titanium alloy substrate by means of physical vapor deposition were investigated.

The findings showed that the highest microhardness value (36.2 GPa) was observed for samples with a (Zr,Hf,Ti)N coating, and the lowest value (12 GPa) - for samples with a (Zr,Nb)N coating. The tribological tests revealed that the friction coefficient values for all coatings was varied in the range of 0.15-0.17. All coatings had a higher coefficient of friction than the substrate material in conditions of used tribological tests. The highest friction coefficient values corresponded to coatings that were characterized by a larger amount of droplet phase on the surface, which may be associated with increased adhesion between the indenter and the metal droplet phase. During scratch testing the highest critical force Lc3 was observed for samples with coatings containing hafnium: (Zr,Hf)N and (Zr,Hf,Ti)N. The (Zr,Hf)N coating also demonstrated the highest value of the critical force Lc2. However, these coatings were characterized by the largest area of chips along the entire length of the track, compared to the other coatings. Coatings containing Nb showed relatively small values of critical loads, which may be associated with the presence of tensile stresses in the ZrN solid solution

The findings showed that the shape of anodic potential dependence on time during electrochemical corrosion tests in galvanostatic mode (3% NaCl environment) strongly dependent on coating type. A sharp growth to the maximum value was characteristic of ZrN, (Zr,Hf)N and (Zr,Nb)N coatings deposited from one cathode, while a gradual growth to the maximum value was observed for (Zr,Ti)N, (Ti,Zr,Hf)N and (Zr,Nb,Ti)N coatings obtained from two cathodes. Such behavior may be explained by the fact that the use of two different cathodes led to the formation of coatings consisting of alternating layers of varied composition. It was shown that the time necessary to reach the maximum stable value of anodic potential could be an indirect parameter of corrosion resistance. (Zr,Nb,Ti)N coating demonstrated the highest value of corrosion resistance according to this criterion that was confirmed by scanning electron microscopy investigations.

Acknowledgements

This work was supported financially by the Belarusian Republican Foundation for Fundamental Research (project no. T23RNF-228) and the Russian Science Foundation (project no. 23-49-10038).

References

Annur, D., Kartika, I., Supriadi, S., Suharno, B., Titanium and titanium based alloy prepared by spark plasma sintering method for biomedical implant applications – a review, *Materials Research Express*, vol. **8**, no. 1, p. 012001, 2021.

Brunello, G., Brun, P., Gardin, C., Ferroni, L., Bressan, E., Meneghello, R., Biocompatibility and antibacterial properties of zirconium nitride coating on titanium abutments: An in vitro study. *PLoS ONE*, vol. **13**, no 6, p. e0199591, 2018.

Chen, H., Feng, R., Xia, T., Wen, Z., Li, Q., Qiu, X., Huang, B., Li, Y., Progress in Surface Modification of Titanium Implants by Hydrogel Coatings. *Gels*, vol. **9**, p. 423, 2023.

Chen, L., Ran, Y., Jiang, Z., Li, Y., & Wang, Z., Structural, Compositional, and Plasmonic Characteristics of Ti–Zr Ternary Nitride Thin Films Tuned by the Nitrogen Flow Ratio in Magnetron Sputtering, *Nanomaterials*, vol. **10**, no. 5, p. 829, 2020.
Chen, Q., Thouas, G. A., Metallic implant biomaterials. *Mater. Sci. Eng. R*, vol. **87**, pp. 1–57, 2015.
Cherenda, N.N., Petukh, A.B., Kuleshov, A.K., Rusalsky, D.P., Bibik, N.V., Uglov, V.V., Grigoriev S.N., Vereschaka, A.A., Astashynski, V.M., Kuzmitski, A.M., Scratch testing of ZrN coating on Ti-6Al-4V titanium alloy surface preliminary treated by compression plasma flows impact, *High Temperature Material Processes*, vol. **28**, no. 3, pp. 25–36, 2024.
Cordeiro, J.M., Barão, V.A.R. Is there scientific evidence favoring the substitution of commercially pure titanium with titanium alloys for the manufacture of dental implants?, *Materials Science and Engineering C*, vol. **71**, pp. 1201-1215, 2017.
Dohm, J.C., Schmidt, S., Puente Reyna, A.L., Richter, B., Santana, A., Grupp, T.M., Comparative Study of Zirconium Nitride Multilayer Coatings: Crystallinity, In Vitro Oxidation Behaviour and Tribological Properties Deposited via Sputtering and Arc Deposition, *J. Funct. Biomater*, vol. 15, p. 223, 2024.
Frank, F., Kainz, C., Tkadletz, M., Czettl, C., Pohler, M., Schalk, N., Microstructural and micro-mechanical investigation of cathodic arc evaporated ZrN/TiN multilayer coatings with varying bilayer thickness, *Surface & Coatings Technology*, vol. **432**, p. 128070, 2022.
Gabor, R., Cvrček, L., Kudrnová, M., Hlinka, J., Večeř, M., Buřil, M., Walter, J., Čekada, M., Drnovšek, A., Unucka, P., Mamulová Kutláková, K., Motyka, O., Seidlerová, J., ZrN coating as a source for the synthesis of a new hybrid ceramic layer, *Applied Surface Science Advances*, vol. **22**, p. 100615, 2024.
Grigoriev, S., Sotova, C., Vereschaka, A., Uglov V., Cherenda, N., Modifying Coatings for Medical Implants Made of Titanium Alloys, *Metals*, vol. 13, p. 718, 2023a.
Grigoriev, S., Vereschaka, A., Uglov, V., Milovich, F., Tabakov, V., Cherenda, N., Andreev, N., Migranov, M., Influence of the tribological properties of the Zr,Hf-(Zr,Hf)N-(Zr,Me,Hf,Al)N coatings (where Me is Mo, Ti, or Cr) with a nanostructured wear-resistant layer on their wear pattern during turning of steel, *Wear*, vol. **518-519**, p. 204624, 2023b.
Gurappa, I., Mechanism of degradation of titanium alloy IMI 834 and its protection under hot corrosion conditions, *Oxidation of metals*, vol. **59**, no. 3, pp. 321–322, 2003.
Huang, J.-H., Kuo, K.-L., Yu, G.-P., Oxidation behavior and corrosion resistance of vacuum annealed ZrN-coated stainless steel, *Surface and Coatings Technology*, vol. **358**, Pages pp. 308-319, 2019.
Kaur, M., Singh, K., Review on titanium and titanium based alloys as biomaterials for orthopaedic applications, *Materials Science and Engineering C*, vol. **102**, pp. 844-862, 2019.
Khorasani, A.M., Goldberg, M., Doeven, E.H., Littlefair, G., Titanium in Biomedical Applications - Properties and Fabrication: a Review, *Journal of Biomaterials and Tissue Engineering*, vol. **5**, pp. 593–619, 2015.
Laera, A.M., Massaro, M., Dimaio, D., Vencl, A., Rizzo, A., Residual Stress and Tribological Performance of ZrN Coatings Produced by Reactive Bipolar Pulsed Magnetron Sputtering, *Materials*, vol. **14**, pp. 6462, 2021.
Lamm, B.W., Mitchell, D.J., Chemical Vapor Deposition of Zirconium Compounds: A Review, *Coatings*, vol. **13**, p. 266, 2023.
Liu, X., Chen, S., Tsoi, J.K.H., Matinlinna, J.P. Binary titanium alloys as dental implant materials – a review, *Regenerative Biomaterials*, vol. **4**, no. 5, pp. 315-323, 2017.
Lotkov, A., Latushkina, S., Kopylov, V., Grishkov, V., Baturin, A., Girsova, N., Zhapova, D., Timkin, V., Nanostructured Coatings (Ti,Zr)N as a Barrier to Hydrogen Diffusion into Ti0.16Pd (wt.%) Alloy, *Metals*, vol. **11**, p. 1332, 2021.
Mohamadian Samim, P., Fattah-alhosseini, A., Elmkhah, H., Imantalab, O., Nanoscale architecture of ZrN/CrN coatings: microstructure, composition, mechanical properties and

electrochemical behavior, *Journal of materials research and technology*, vol. **15**, pp. 542 – 560, 2021.
Nouri, A., Wen C,. Introduction to surface coating and modification for metallic biomaterials, in *Surface Coating and Modification of Metallic Biomaterials*, C. Wen, Ed., Cambridge: Woodhead Publishing, pp. 3-60, 2015.
Pogrebnjak, A., Ivashchenko, V., Bondar, O., Beresnev, V., Sobol, O., Załęski, K., Jurga, S., Coy, E., Konarski, P., Postolnyi, B., Multilayered vacuum-arc nanocomposite TiN/ZrN coatings before and after annealing: Structure, properties, first-principles calculations, *Materials Characterization*, vol. **134**, pp. 55-63, 2017.
Rabadzhiyska, S., Dechev, D., Ivanov, N., Ivanova, T., Strijkova, V., Katrova, V., Rupetsov, V., Dimcheva, N., Valkov, S., Wear and Corrosion Resistance of ZrN Coatings Deposited on Ti6Al4V Alloy for Biomedical Applications, *Coatings*, vol. **14**, p. 1434, 2024.
Randall, N.X., The current state-of-the-art in scratch testing of coated systems, *Surface and Coatings Technology*, vol. **380**, p. 125092, 2019.
Sarraf, M., Rezvani Ghomi, E., Alipour, S., Ramakrishna, S., Liana Sukiman, N., A state-of-the-art review of the fabrication and characteristics of titanium and its alloys for biomedical applications, *Bio-Design and Manufacturing*, vol. **5**, no. 2, pp. 371-395, 2022.
Tang, J., Liu, D., Zhang, X., Du, D., Yu, S., Effects of Plasma ZrN Metallurgy and Shot Peening Duplex Treatment on FrettingWear and Fretting Fatigue Behavior of Ti6Al4V Alloy, *Materials*, vol. **9**, p. 217, 2016.
Vereschaka, A., Tabakov, V., Grigoriev, S., Sitnikov, N., Milovich, F., Andreev, N., Sotova, C., Kutina, N., Investigation of the influence of the thickness of nanolayers in wear-resistant layers of Ti-TiN-(Ti,Cr,Al)N coating on destruction in the cutting and wear of carbide cutting tools. *Surf. Coat. Technol*., vol. **385**, p. 125402, 2020.
Vereschaka, A., Cherenda, N., Sotova, C., Uglov, V., Reva, O., Basalai, A., Isobello, A., Baranova, N., Development of Multicomponent Nanostructured Nitride Coatings to Protect against Corrosion Products from Titanium Alloy, *Coatings*, vol. **13**, p. 2028, 2023.
Wu, Z., Gao, Z., Zhao, J., Li, S., Hao, Q., Ran, S., Enhanced Mechanical Properties of Yellow ZrN Ceramic with Addition of Solid Solution of TiN, *Materials*, vol. **15**, p. 7866, 2022.